BIOCHEMISTRY
including biophysical chemistry & molecular biology
Article

Biochemistry **2009,** *48,* 8965–8975 8965
DOI: 10.1021/bi900759v

Multiple Protonation States of Vesicular Acetylcholine Transporter Detected by Binding of [^{3}H]Vesamicol[†]

Parul Khare, Aubrey R. White, and Stanley M. Parsons*

Department of Chemistry and Biochemistry, Neuroscience Research Institute, University of California, Santa Barbara, California 93106

Received May 3, 2009; Revised Manuscript Received August 13, 2009

ABSTRACT: Vesicular acetylcholine transporter (VAChT) is inhibited by (−)-vesamicol [(−)-*trans*-2-(4-phenylpiperidino)cyclohexanol], which binds tightly to an allosteric site. The tertiary alkylamine center in (−)-vesamicol is protonated and positively charged at acidic and neutral pH and unprotonated and uncharged at alkaline pH. Deprotonation of the amine has been taken to explain loss of (−)-vesamicol binding at alkaline pH. However, binding data deviate from a stereotypical bell shape, and more binding occurs than expected at alkaline pH. The current study characterizes the binding of (−)-vesamicol from pH 5 to pH 10 using filter assays, (−)-[^{3}H]vesamicol (hereafter called [^{3}H]vesamicol), and human VAChT expressed in PC12$^{A123.7}$ cells. At acidic pH, protons and [^{3}H]vesamicol compete for binding to VAChT. Preexposure or long-term exposure of VAChT to high pH does not affect binding, thus eliminating potential denaturation of VAChT and failure of the filter assay. The dissociation constant for the complex between protonated [^{3}H]vesamicol and VAChT decreases from 12 nM at neutral pH to 2.1 nM at pH 10. The simplest model of VAChT that explains the behavior requires a proton at site 1 to dissociate with pK_1 = 6.5 ± 0.1, a proton at site A to dissociate with pK_A = 7.6 ± 0.2, and a proton at site B to dissociate with pK_B = 10.0 ± 0.1. Deprotonation of the site 1 proton is obligatory for [^{3}H]vesamicol binding. Deprotonation of site A decreases affinity (2.2 ± 0.5)-fold, and deprotonation of site B increases affinity (18 ± 4)-fold. Time-dependent dissociation of bound [^{3}H]vesamicol is biphasic, but equilibrium saturation curves are not. The contrasting phasicity suggests that the pathway to and from the [^{3}H]vesamicol binding site exists in open and at least partially closed states. The potential significance of the findings to development of PET and SPECT ligands based on (−)-vesamicol for human diagnostics also is discussed.

Vesicular acetylcholine transporter (VAChT)[1] moves the neurotransmitter acetylcholine (ACh) from the cytoplasm of nerve terminals to the inside of synaptic vesicles (*1*, *2*). It belongs to the major facilitator superfamily (MFS) of transporters, most of which contain 12 transmembrane (TM) helices (*3*). Three-dimensional structures for four bacterial members of the MFS have been determined. They are lactose permease (*4*), glycerol phosphate transporter (*5*), oxalate−formate antiporter (*6*), and the multidrug resistance transporter EmrD (*7*). The structures all exhibit similar TM nearest neighbors (*4*−*6*). The first six TMs in the amino acid sequence pack into one bundle, and the second six TMs pack into another bundle. The bundles are related to each other by a pseudo-2-fold axis running through a central transport channel approximately perpendicular to the plane of the membrane. TM 1 is pseudosymmetric to TM 7, TM 2 to TM 8, and so on. Similar architecture is hypothesized to apply to most MFS proteins, including VAChT (*8*). Accordingly, a three-dimensional homology model of VAChT based on the three-dimensional structure of glycerol-3-phosphate transporter and biochemical information about VAChT has been proposed (*9*). In the model, the ACh transport channel is open to cytoplasm and closed to vesicular lumen. This orientation constitutes >90% the "resting" conformation of VAChT *in vitro* (*10*).

Protonmotive force generated by V-ATPase, which also is in the vesicular membrane, drives transport of ACh (*10*). Thus, VAChT must contain functional proton-binding sites that mediate efflux of protons through the protein. The synthetic compound (−)-vesamicol [(−)-*trans*-2-(4-phenylpiperidino)cyclohexanol] binds tightly to VAChT and inhibits transport (*11*). The structure−function relationship for (−)-vesamicol is restrictive, which implies that the compound makes specific contacts with a selective binding site (*11*). Mutational analysis has localized the likely (−)-vesamicol binding site near residue D398, which faces the transport channel near the center of TM 10 (*12*, *13*). Residue numbers used throughout this report apply to rat and human VAChT. The ACh binding site probably is immediately adjacent to the (−)-vesamicol binding site and closer to vesicular lumen (*14*). A rocker-switch model of transport by the MFS has been proposed (*8*). The two bundles of TMs are hypothesized to rock against each other along the transport

[†]This research was supported by Grant NS15047 from the National Institute of Neurological Disorders and Stroke, NIH.

*To whom correspondence should be addressed. E-mail: parsons@chem.ucsb.edu. Telephone: (805) 893-2252. Fax: (805) 893-4120.

[1]Abbreviations: (±)-ABV, (±)-aminobenzovesamicol; ACh, acetylcholine; AMPSO, *N*-(1,1-dimethyl-2-hydroxyethyl)-3-amino-2-hydroxypropanesulfonic acid; HEPES, 4-(2-hydroxyethyl)-1-piperazineethanesulfonic acid; MES, 2-(*N*-morpholino)ethanesulfonic acid; MFS, major facilitator superfamily; TM, transmembrane segment; UBB, uptake binding buffer; VAChT, vesicular acetylcholine transporter; hVAChT, human VAChT; VMAT, vesicular monoamine transporter; [^{3}H]vesamicol, (−)-[^{3}H]vesamicol and (−)-[^{3}H]-*trans*-2-(4-phenylpiperidino)cyclohexanol; (±)-vesamicol, (±)-*trans*-2-(4-phenylpiperidino)cyclohexanol; (−)-vesamicol, (−)-*trans*-2-(4-phenylpiperidino)cyclohexanol.

Published on Web 08/17/2009

channel in order to expose the substrate-binding site to first one side and then the other side of the membrane (*7*, *15*). For VAChT, protons trigger the rocking.

Equilibrium binding of (−)-vesamicol across the accessible pH range is very approximately bell-shaped, with zero binding at both low and high values of pH (*12*, *16*). When a pH-binding curve is truely bell-shaped, only two weak acids control the profile (*17*). One acid has a p*K* value in the lower pH range. It must dissociate to allow ligand binding. A different weak acid has a p*K* value in the higher pH range. It must not dissociate for ligand binding. Only in the midrange of pH are both conditions for binding well satisfied.

Critical weak acids can be associated with *either* the protein *or* the ligand, and a pH-binding profile will look the same. Because (−)-vesamicol is a tertiary alkylamine, it is protonated and positively charged at acidic and neutral pH values but unprotonated at alkaline pH values. Protonated (−)-vesamicol probably is the binding form, as (−)-vesamicol binds tightly at neutral pH but weakly at alkaline pH. Also, methylation of the tertiary amine in (±)-vesamicol decreases affinity ≥25-fold, indicating that a proton bound to the amine center is important (*18*). The pK_{aves} value for protonated (−)-vesamicol is 9.0 ± 0.1, which has been determined by titration of (±)-vesamicol absorbance at 263 nm (*19*). In the absence of other effects, the apparent affinity of VAChT for (−)-vesamicol is predicted to decrease by 91% at pH 10.0. In past analyses, we assumed that deprotonation of (−)-vesamicol fully explains the high-pH limb of the pH-binding profile. However, data persistently deviate from the simple titration curve expected. The deviation must arise from the presence in VAChT of one or more important weak acids having p*K* values in the mildly alkaline pH range. Because such weak acids might participate in transport, we carefully reevaluated the pH-binding profile for (−)-vesamicol.

MATERIALS AND METHODS

All chemical reagents were of the highest usual grades commercially available. The radioactive compound (−)-[^{3}H]vesamicol (25 Ci/mmol) was custom synthesized by Perkin-Elmer Corp. In the interest of brevity, the term [^{3}H]vesamicol means the tritiated, potent (−)-enantiomer. The term (−)-vesamicol means the nonradioactive (−)-enantiomer, and the terms (±)-vesamicol and (±)-aminobenzovesamicol [(±)-ABV] mean the nonradioactive racemates. The compounds (±)-ABV, (±)-vesamicol hydrochloride, and (−)-vesamicol hydrochloride were synthesized in this laboratory (*18*). PC12$^{A123.7}$ cells were from L. B. Hersh (University of Kentucky, Lexington, KY).

Cell Line. The PC12$^{A123.7}$ cell line does not express endogenous rat VAChT (*20*). It contains synaptic-like microvesicles to which transfected VAChT is targeted (*21*). Cells were grown at 37 °C in an atmosphere of 10% CO_2 in complete Dulbecco's modified Eagle's medium mixed 1:1 with Ham's F-12 medium. The culture medium was supplemented with 10% horse serum, 5% fetal bovine serum, 100 units of penicillin/mL, and 100 μg of streptomycin/mL.

Stable Transfection. cDNA for human VAChT (hVAChT) was obtained from Invitrogen and transferred into pcDNA 6.2/V5-destination vector using the LR recombinase method (Invitrogen). Clones of recombinant vector (hVAChT/pcDNA 6.2/V5) were obtained in XL-1 Blue supercompetent *Escherichia coli* cells selected on ampicillin and amplified. Isolated hVAChT/pcDNA 6.2/V5 was transfected into PC12$^{A123.7}$ cells with lipofectamine in antibiotic-free medium (*22*). Twenty-four hours later, cells were passaged at different dilutions in different culture plates, and blasticidin selection agent was added at 10 μg of blasticidin/mL to each plate. Blasticidin-resistant colonies were picked after 2−3 weeks, expanded and maintained in a culture medium containing blasticidin in addition to 5% horse serum, 10% fetal bovine serum, 100 units of penicillin/mL, and 100 μg of streptomycin/mL.

Preparation of Postnuclear Supernatant. Cells were trypsinized and harvested upon growth to confluency, washed with cold phosphate-buffered saline, and resuspended in homogenization buffer [0.32 M sucrose, 10 mM *N*-(2-hydroxyethyl)piperazine-*N*′-2-ethanesulfonic acid (HEPES), 1 mM dithiothreitol, adjusted to pH 7.4 with KOH, fresh 100 μM phenylmethanesulfonyl fluoride (Sigma, St. Louis, MO), 100 μM diethyl *p*-nitrophenyl phosphate (paraoxon), and complete protease inhibitor cocktail (Roche, Mannheim, Germany)]. Homogenate was prepared (*22*). Briefly, resuspended cells were broken in a Potter-Elvehjam homogenizer (three to six strokes) using a motor-driven stirrer until 95% of them took up trypan blue as determined by microscopic examination. The resulting suspension was centrifuged at 1500*g* for 10 min, and the postnuclear supernatant was reserved. Protein concentration was estimated with the Bradford assay (Bio-Rad, Hercules, CA). It typically was about 10 mg/mL (*23*). Different preparations of postnuclear supernatant contain different amounts of hVAChT/mg of protein.

Western Blot Analysis and Selection of Clonal Line. Expression of hVAChT by each of the clones was monitored by Western blot (*22*). Postnuclear supernatant (150 μg) was diluted to 500 μL with homogenization buffer containing complete protease inhibitor cocktail and pelleted by ultracentrifugation at 171500*g* for 1.5 h at 4 °C. The pellet was resuspended in 40 μL of sodium dodecyl sulfate sample buffer (New England BioLabs, Beverly, MA) containing 0.042 M dithiothreitol. Proteins were separated by electrophoresis on a 12% resolving and 4% stacking sodium dodecyl sulfate−polyacrylamide gel and blotted onto an Invitrolon polyvinylidene fluoride membrane (Invitrogen) using a semidry electrotransfer apparatus (Mini-Trans blot cell; Bio-Rad). The membrane was blocked with Tris-buffered saline containing 2.5% nonfat milk and 0.05% Tween 20 for 1 h at 23 °C, followed by overnight incubation with polyclonal goat antibody raised against the N-terminus of hVAChT (Santa Cruz Biotechnology, Santa Cruz, CA). The membrane was rinsed and then incubated for 1 h with horseradish peroxidase-conjugated donkey anti-goat IgG (Santa Cruz Biotechnology) at 23 °C. Electrochemiluminescent detection was performed using a standard kit (Pierce Chemical Co.) as instructed by the manufacturer.

pH-Binding Profile for [^{3}*H*]*Vesamicol*. The different pH values were achieved as described (*12*). In brief, a solution of 2-(*N*-morpholino)ethanesulfonic acid (MES)/HEPES/3-[(1,1-dimethyl-2-hydroxyethyl)amino]-2-hydroxypropanesulfonic acid (AMPSO), each at 99.6 mM and containing 4 mM fresh dithiothreitol, is pH 4.5 and 291 mOsm/kg. A similar solution of MES/HEPES/AMPSO, each at 58.3 mM, containing 4 mM fresh dithiothreitol and adjusted to pH 11.0 with KOH, is 306 mOsm/kg. These low- and high-pH, nearly isoosmolal stock solutions were mixed with each other in different proportions to obtain intermediate pH values (pH buffer). Postnuclear supernatant (< 50 μL) containing 20 μg of protein and the volume of homogenization buffer required to sum to 50 μL were added to 100 μL of pH buffer. Incubation for 10 min and 23 °C was initiated by the addition of 50 μL of a solution containing uptake

binding buffer (UBB) [110 mM potassium tartrate, 20 mM HEPES (pH 7.4 with KOH), and 1 mM dithiothreitol] and 20 nM [^{3}H]vesamicol. The pH of each incubation was measured shortly before filtration. Eighty-five microliters of each solution was applied to a filter prewetted immediately before with ice-cold wash buffer [UBB containing 5 μM (±)-vesamicol], and unbound radioactivity was immediately washed through with four 1 mL volumes of ice-cold wash buffer. The (±)-vesamicol in wash buffer prevented free [^{3}H]vesamicol from binding to VAChT during filtration. A second 85 μL portion obtained from the same incubation mixture also was filtered and washed. Radioactivity on the filters was determined with liquid scintillation spectrometry to an uncertainty of ≤2% in cpm, and results were averaged. This procedure was repeated for each pH value. Nonspecific binding was measured at several pH values in the presence of 5 μM (±)-vesamicol. Inclusion of the protonophore nigericin (100 nM) did not affect the pH-binding profile.

Saturation Curves for [^{3}H]Vesamicol. They were acquired similarly to the procedure described above in two groups. In one group, the pH values were 5.0, 5.5, 6.0, 6.5, and 6.9. In the other group, the pH values were 7.1, 7.6, 8.0, 8.9, 9.3, and 10.0. Incubation in the stated concentrations of [^{3}H]vesamicol was for 10 min at 37 °C. Bound [^{3}H]vesamicol was determined by filtration as described above. Nonspecific binding was determined with 100 nM (±)-ABV.

Time-Dependent Dissociation of [^{3}H]Vesamicol. This was characterized at pH values ranging from 7.3 to 9.5. Three hundred micrograms of postnuclear supernatant was mixed with pH buffer to yield a final volume of 1350 μL containing 100 nM nigericin. Reaction at 23 °C was initiated by addition of 75 μL of UBB containing 100 nM [^{3}H]vesamicol. Incubation was continued for 20 min, after which bound [^{3}H]vesamicol was determined as described above. This datum estimated binding at t = 0. Seventy-five microliters of 100 μM (±)-vesamicol was added at t = 0. Bound [^{3}H]vesamicol was determined as described above at times ranging from 10 s to 45 min. The amount of bound [^{3}H]vesamicol in each sample was normalized to the amount of protein filtered. Nonspecific binding was determined in the presence of 5 μM (±)-vesamicol.

Stability of hVAChT at High pH. Postnuclear supernatant (500 μg) was mixed with UBB at pH 7.6 to yield a final volume of 49 mL containing 100 nM nigericin. Incubation was initiated by addition of 1000 μL of UBB containing 200 nM [^{3}H]vesamicol. Bound [^{3}H]vesamicol was determined as described above at times ranging from 10 s to 19 min. At 20 min, 5320 μL of 0.5 M AMPSO brought to pH 10.5 with KOH and containing 4 nM [^{3}H]vesamicol was quickly mixed with the reaction to raise the pH to 9.6. Bound [^{3}H]vesamicol was determined as described above at times ranging from 10 s to 19 min after AMPSO was added. At 40 min total elapsed time, 4340 μL of 0.50 M MES at a pH of 3.5 was added to bring the pH to 7.4. Bound [^{3}H]vesamicol was determined by filtration as described above at times ranging from 10 s to 20 min after MES was added. The amount of bound [^{3}H]vesamicol in each sample was normalized to the amount of protein filtered. Nonspecific binding was measured in the presence of 5 μM (±)-vesamicol.

Regression, Statistical Analysis, and Simulation. Regression was performed by simultaneously fitting appropriate equations to total and nonspecific binding with the software Scientist (Micromath Research, St. Loius, MO). The best-fit values for nonspecific binding were subtracted from the data for total binding in order to present the less cluttered fits to specific binding shown in Figures 3, 4, and 6. Quoted errors are ±1 standard deviation. The results included calculation of a model selection criterion (based on the Akaike information criterion), which estimates goodness of fit adjusted for the number of degrees of freedom. All fits exhibit high scores in the model selection criterion. The simulations in Figure 8 were conducted with Scientist.

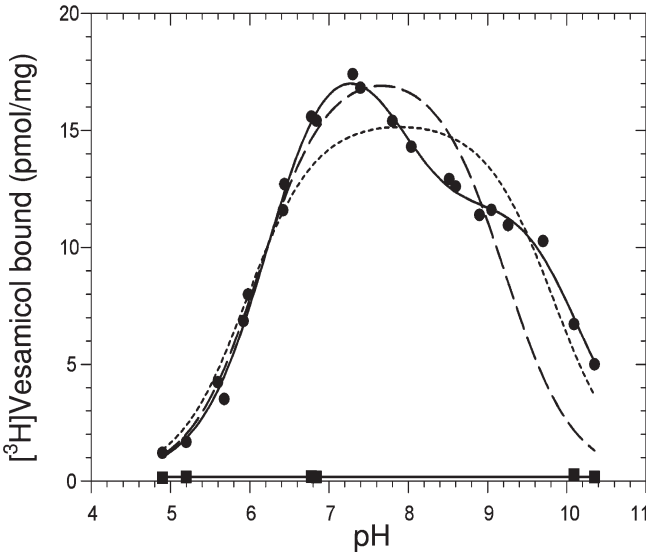

FIGURE 1: pH profile for [^{3}H]vesamicol binding. Low, subsaturating concentrations of postnuclear supernatant (20 μg/mL) and [^{3}H]vesamicol (5 nM) were incubated for 10 min. The amounts of total (●) and nonspecific (■) binding at the indicated pH values are shown. At pH values increasing from ~5 to 7.4, [^{3}H]vesamicol binding increases smoothly in a stereotypical manner. Above pH ~7.4, binding decreases with a concave-up character to the profile at pH ~8.5 and a pronounced shoulder above pH ~9. Three models for protonation of VAChT (i, – –; ii, - - -; and iii, —) are explained in the text. Four other experiments gave similar results. See Appendix 2 for the regression equation corresponding to successful model iii and Table 1 for the parameter values averaged from all experiments.

RESULTS

Erickson and Varoqui (*24*) were the first to report ACh transport by VAChT expressed from cDNA transfected into PC12 cells. However, this cell line makes a low level of endogenous rat VAChT. In the current work, we expressed hVAChT in a derivative of PC12 cells termed PC12$^{A123.7}$ that makes no VAChT. The PC12$^{A123.7}$ cell line removes the possibility that complexity in [^{3}H]vesamicol binding properties arises from a mixture of VAChT species (*20*).

pH Profile for Binding of [^{3}H]Vesamicol. Binding was determined at a low concentration of [^{3}H]vesamicol and a low concentration of hVAChT so that only a small fraction of each is bound to the other. This condition allows simplified analysis of the data. The profile for the amount of [^{3}H]vesamicol binding versus pH in the acidic region has a simple, classical shape, whereas the profile in the alkaline region does not, as a shoulder of binding is present around pH 9.5 (Figure 1). The deviation would be missed if the [^{3}H]vesamicol concentration were saturating, as the full profile would exhibit a plateau amount of binding (namely, B_{max}) over the entire intermediate pH range. The plateau would be quite broad, as the two transition regions between zero and B_{max} binding would spread apart toward lower and higher pH regions.

Competition between Protons and [^{3}H]Vesamicol at Acidic pH. A decrease in binding of [^{3}H]vesamicol at acidic

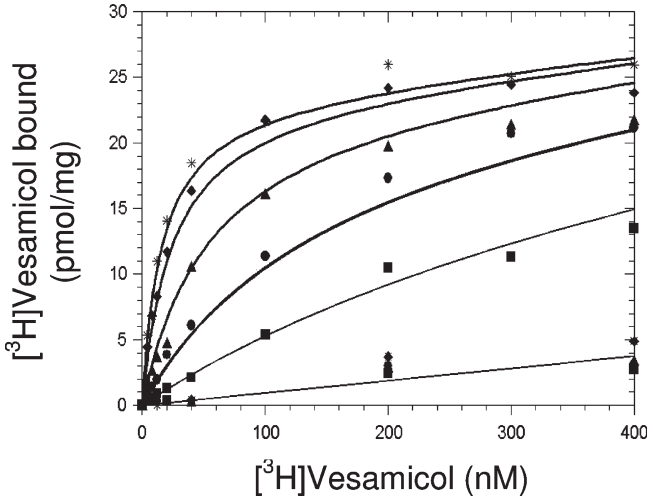

FIGURE 2: Saturation curves for total and nonspecific binding of [^{3}H]vesamicol at acidic pH values. The indicated concentrations of [^{3}H]vesamicol were incubated with postnuclear supernatant (20 μg/mL) at pH 5.0 (■), 5.5 (●), 6.0, (▲), 6.5 (◆), and 6.9 (*). The amounts of total and nonspecific binding are shown using the same symbols, with nonspecific data associated with the single straight line at the bottom. The equation nonspecific binding = slope × V was fitted to the pooled data for nonspecific binding, and the equation total binding = $B_{max}V/(V + K_{dves}(1 + 10^{-pH}/10^{-pK_1})) +$ slope × V was fitted simultaneously to each data set for total binding at each pH value. V is the concentration of free [^{3}H]vesamicol, K_{ves} is the apparent (−)-vesamicol dissociation constant (not precisely the same as K_{dves}), and pK_1 applies to a weak acid in VAChT that must dissociate to allow binding of [^{3}H]vesamicol. Parameter values were B_{max} = 23.6 ± 0.43 pmol/mg, K_{ves} = 10.1 ± 1.15 nM, and pK_1 = 6.63 ± 0.06.

pH has been observed before for rat and *Torpedo* VAChTs (*10*, *16*, *25*). We characterized the type of competition occurring between protons and [^{3}H]vesamicol (that is, competitive or noncompetitive) in hVAChT by determining the saturation curves at different pH values in the acidic range (Figure 2). A competitive model fits the data well, with an apparent dissociation constant for [^{3}H]vesamicol of 10.1 ± 1.15 nM and pK_1 = 6.63 ± 0.06 for a weak acid that must dissociate to bind [^{3}H]vesamicol. This simplified competition model works well because the complexities of the system in the alkaline pH region (below) are minor in the acidic pH region.

VAChT Stability at Alkaline pH. Most proteins and lipids are more sensitive to damage by alkaline pH than acidic pH. Before accepting the anomalies in the basic region of the pH-binding profile as real, several tests for damage were conducted. To test the possibility that irreversible denaturation occurs, VAChT bound to a low concentration of [^{3}H]vesamicol was cycled from about neutral pH to high pH to about neutral pH (Figure 3). Initial binding at pH 7.4 required ~10 min to reach equilibrium. At 20 min the pH was raised to 9.6, and some of the bound [^{3}H]vesamicol rapidly dissociated with a rate constant of about 2.8 ± 1.1 min^{-1}, after which binding was stable at a new, lower level for at least 20 min. The decrease in binding is consistent with the data shown in Figure 1. The pH was returned to 7.4, and the original amount of binding returned at a rate similar to that observed for the initial binding at pH 7.4. Thus, exposure to pH 9.6 for 20 min caused no discernible change in the [^{3}H]vesamicol binding properties of hVAChT.

[^{3}H]Vesamicol Binding Curves Using (±)-Aminobenzovesamicol [(±)-ABV] To Block Specific Binding at Alkaline pH. To characterize hVAChT stability further, saturation

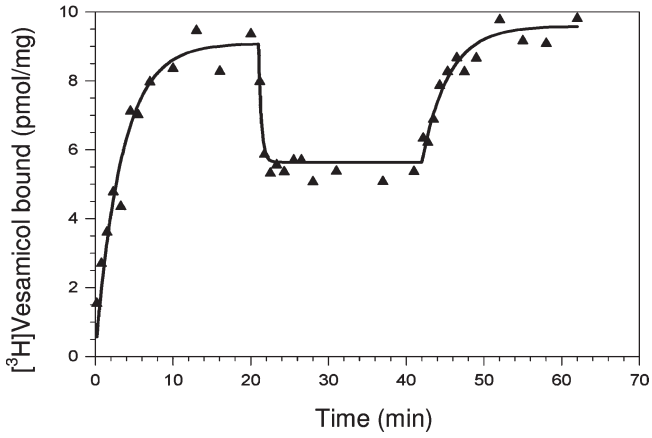

FIGURE 3: Test of hVAChT stability at alkaline pH. Vesicles were incubated in 100 nM nigericin to prevent formation of pH gradients. A low concentration of [^{3}H]vesamicol (4 nM) was added at pH 7.4 and 0 min, and it was maintained at 4 nM throughout the experiment. The pH was rapidly raised to 9.6 at 20 min and held there for 19 min. The pH was rapidly lowered to 7.4 for another 19 min. A time course utilizing exponential transitions was fitted to the data.

titrations were carried out at different alkaline pH values. However, there is a problem. Saturation titrations utilizing as much as 1 μM [^{3}H]vesamicol require 200 μM (±)-vesamicol (a 100-fold excess of the potent enantiomer) to block specific binding. Because most of it is unprotonated, 200 μM (±)-vesamicol is not soluble at pH 10 (data not shown). Inadequate solubility is not a problem for the other experiments reported here, as 1 mM (±)-vesamicol is soluble at acidic and neutral pH, and 5 nM [^{3}H]vesamicol is soluble at alkaline pH. Luckily, an analogue of (±)-vesamicol abbreviated (±)-ABV is about 1000-fold more potent than (±)-vesamicol is, and it is soluble at pH 10 in the concentration required to completely block specific binding of 1 μM [^{3}H]vesamicol (*26*).

Single rectangular hyperbolas fit all data sets at all alkaline pH values using (±)-ABV to determine nonspecific background. The B_{max} values obtained when data sets were fitted independently were within errors of each other (not shown). Thus, [^{3}H]vesamicol binding is stable to alkaline pH values, and the filters quantitatively capture membranes up to pH 10.0. In the final round of regression, a single B_{max} value was assumed for all pH values, and only protonated [^{3}H]vesamicol was assumed to bind (Figure 4, Appendix 1). The dissociation constant for protonated [^{3}H]vesamicol (K^{pH}_{dves}) varies from 12.5 ± 1.6 to 9.1 ± 1.1 from pH 7.1 to pH 8.9. Above pH 8.9, K^{pH}_{dves} decreases to 2.1 ± 0.3 (Table 2). In other words, binding of protonated [^{3}H]vesamicol tightens substantially at pH ~10.

Does [^{3}H]Vesamicol Exhibit "Specific" Binding to Membranes Containing No VAChT? Even membranes not containing VAChT might bind displaceable [^{3}H]vesamicol. For example, (−)-vesamicol binds to sigma 1 and 2 receptors with affinities only somewhat less than for VAChT (*27*). PC12 cells contain very little of sigma receptors, but other non-VAChT binding sites for [^{3}H]vesamicol might be present (*28*). Such binding could have its own pH dependence that might complicate apparent pH dependence of VAChT. Thus, a postnuclear supernatant was prepared from cells not transfected with VAChT, and the pH profiles for total and nonspecific binding of [^{3}H]vesamicol were determined. Five nanomolar [^{3}H]vesamicol produces essentially no "specific−nonspecific" binding at low pH, but it produces ~0.4 pmol/mg at high pH. A fit to the pH dependence

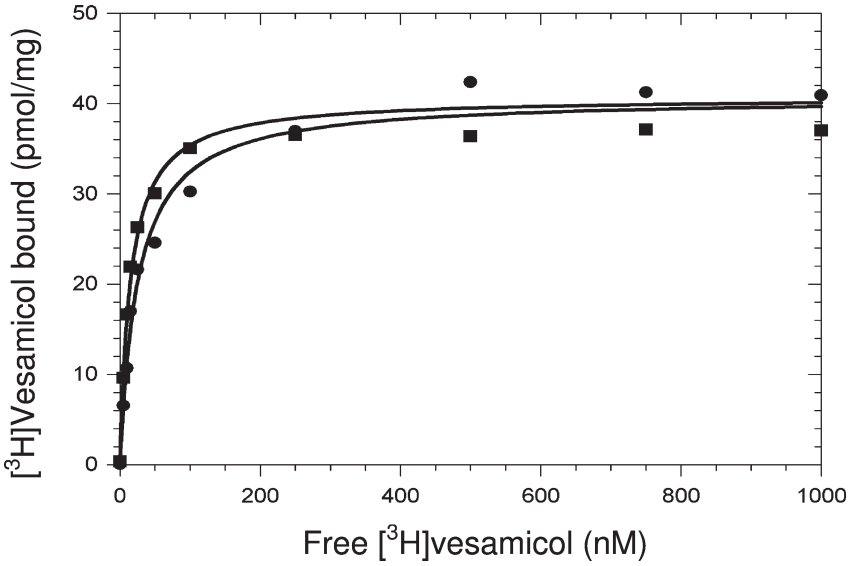

FIGURE 4: Selected saturation curves for specific binding of [^{3}H]vesamicol at alkaline pH. A simultaneous fit of the equations given in Appendix 1 to data for binding of 4 nM hVAChT at pH 7.1, 7.6, 8.0, 8.9, 9.3, and 10.0 was carried out. The same B_{max} value was assumed for all pH values (40.4 ± 0.5 pmol of hVAChT/mg). Only the data and fit at pH 7.1 (■) and pH 10.0 (●) are shown because of graphical clutter when all data are shown. The concentration of free [^{3}H]vesamicol on the *x*-axis is the total concentration (protonated + unprotonated). The K_{dves}^{pH} value obtained for binding of protonated [^{3}H]vesamicol at each pH is listed in Table 2.

yields a pK value of ~7.3. The amplitude at high pH saturates at higher concentrations of [^{3}H]vesamicol (not shown). As it is quantitatively very little under all conditions utilized here, specific−nonspecific binding can be ignored.

Development of a VAChT Protonation Model. The tests for artifacts being negative, three models for weak acids linked to the [^{3}H]vesamicol binding site were fitted to the data (see Appendix 2 for equations describing the successful model). The models started with the simplest possible and increased in complexity by introducing terms required to reproduce the anomalous binding features. All models assume that protonation of a single amino acid residue in VAChT we call site 1 and deprotonation of [^{3}H]vesamicol itself completely block binding (*19*). The former assumption is supported by the competitive relationship with protons (Figure 2). The latter assumption is in a strict sense not proven, but it is by far the simplest possibility consistent with data. Model i makes no other assumption. Model ii assumes in addition that deprotonation of another residue in VAChT we call site B increases [^{3}H]vesamicol affinity, as required to account for the shoulder of excess binding at and above pH ~9.5. Model iii incorporates model ii with the additional assumption that deprotonation of yet another residue in VAChT we call site A decreases [^{3}H]vesamicol affinity. This event is required to account for the concave-up character to the profile at pH ~8.5.

Models i and ii provide poor fits to the data, but model iii provides an excellent fit (Figure 1). Figure 5 shows the protonation states of VAChT and [^{3}H]vesamicol hypothesized by model iii. The required parameters are pK_1, pK_A, α (the factor by which K_A for site A changes when [^{3}H]vesamicol is bound), pK_B, β (the factor by which K_B for site B changes when [^{3}H]vesamicol is bound), and K_{dves} (the pH-independent constant for dissociation of $VH^+ \cdot VAChT \cdot H_A^+ \cdot H_B^+$, where VH^+ is protonated [^{3}H]vesamicol). The averaged values for the parameters obtained from five determinations of the pH-binding profile are given in Table 1. These values are in close agreement with those of the independent experiments reported in Figure 2 and Table 2.

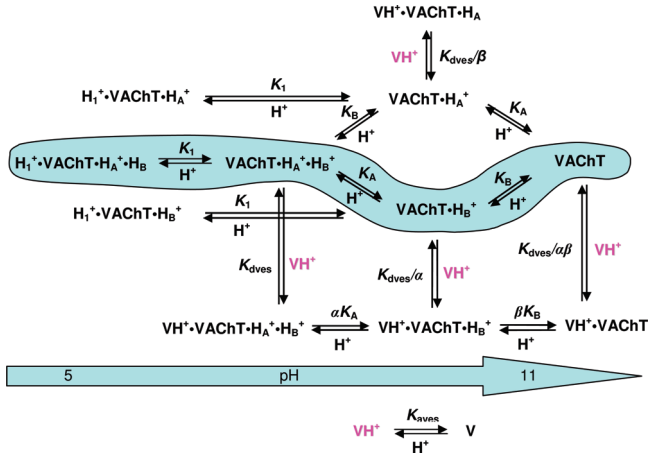

FIGURE 5: Hypothesized hVAChT protonation states. $H_1^+ \cdot VAChT \cdot H_A^+ \cdot H_B^+$ is VAChT protonated at sites 1, A, and B. The sites are assumed to be independent of each other, and only the protonated (VH^+, in hot pink) and not unprotonated (V) form of [^{3}H]vesamicol can bind. The acid dissociation constant for VH^+ is $K_{aves} = 10^{-pK_{aves}} = 10^{-9.0}$. The most populated states of VAChT not bound to protonated [^{3}H]vesamicol, moving left to right from acidic to basic pH, as indicated by the light blue arrow, are circled and highlighted with light blue. Bound H_1^+ dissociates from site 1 with constant K_1 to allow VH^+ binding. K_{dves} is the "pH-independent" constant for VH^+ dissociation from $VH^+ \cdot VAChT \cdot H_A^+ \cdot H_B^+$. The proton H_A^+ dissociates from site A in free VAChT with acid dissociation constant K_A. When [^{3}H]vesamicol is bound, the acid dissociation constant is αK_A. When H_A^+ is dissociated, the [^{3}H]vesamicol dissociation constant is K_{dves}/α by thermodynamic linkage. H_B^+ dissociates from site B in free VAChT with acid dissociation constant K_B. When [^{3}H]vesamicol is bound, the acid dissociation constant is βK_B. When H_B^+ is dissociated, the [^{3}H]vesamicol dissociation constant is K_{dves}/β by thermodynamic linkage. The regression equations corresponding to the scheme are derived in Appendix 2. Parameter values are listed in Table 1.

Interpretation of the parameter values is presented next. Dissociation of site 1 having pK_1 = 6.5 ± 0.1 is required for any binding of [^{3}H]vesamicol. Dissociation of site A having pK_A = 7.6 ± 0.2 decreases affinity for protonated [^{3}H]vesamicol

by (2.2 ± 0.5)-fold (that is, α = 0.45 ± 0.11), which is a modest amount. Existence of site A is consistent with the small changes in K_{dves} seen from pH 7.1 to pH 8.9, as site 1 and site A significantly cancel their effects on [^{3}H]vesamicol affinity in this pH range (Table 2). Dissociation of site B having pK_B = 10.0 ± 0.1 increases affinity for [^{3}H]vesamicol by (18 ± 4)-fold (that is, β = 18 ± 4), which is a large amount. It is consistent with the substantial decrease in K_{dves}^{pH} seen from pH 8.9 to pH 10.0 (Table 2).

Time Dependence for Dissociation of Bound [^{3}H]Vesamicol. To further test whether bound [^{3}H]vesamicol is in different environments at alkaline and neutral pH values, which the factors α and β imply, time-dependent dissociation was characterized. About 73−80% of the dissociation occurs ~7.5-fold faster than the remaining dissociation at all alkaline pH values (Figure 6 and Table 3). Apparently, sites A and B do not couple to the process controlling the fractions of fast and slow dissociation. The value of the k_{fast} rate constant at pH 9.5 (2.27 ± 0.25 min^{-1}), determined after addition of excess (±)-vesamicol, is similar to that of the rate constant determined after jumping to pH 9.6 (2.8 ± 1.1 min^{-1}). Thus, dissociation occurs at similar rates regardless of how it is induced.

The values of the faster and slower rate constants increase by a factor of 4 from pH 7.3 to pH 9.5. The increase presumably is not due to long-range electrostatic effects. Higher pH increases negative charge on the protein, which has a predicted pI of 5.69 (*29*). This effect will stabilize bound, positively charged [^{3}H]vesamicol. Because high pH instead destabilizes bound [^{3}H]vesamicol, as indicated by the faster dissociation rates, the binding site has properties at alkaline pH different from those at neutral pH.

Table 1: Equilibrium Binding of Protons and [^{3}H]Vesamicol to hVAChT[a]

parameter	value	parameter	value
pK_1	6.5 ± 0.1	K_{dves} (nM)[b]	15.1 ± 1.6
pK_A	7.6 ± 0.2	pK_B	10.0 ± 0.1
pK_A^{ves}	7.9 ± 0.3	pK_B^{ves}	8.7 ± 0.4
α[c]	0.45 ± 0.11	β[d]	18 ± 4

[a]Data shown in Figure 1 were fitted by the scheme shown in Figure 5 and the equations developed in Appendix 2. [b]Equilibrium dissociation constant for binding of protonated [^{3}H]vesamicol to VAChT·H_A^+·H_B^+. [c]Factor by which the acid dissociation constant K_A changes (to αK_A) when [^{3}H]vesamicol is bound. The dissociation constant K_{dves} for bound [^{3}H]vesamicol becomes K_{dves}/α when site A is deprotonated. [d]Factor by which the acid dissociation constant K_B changes (to βK_B) when [^{3}H]vesamicol is bound. The dissociation constant K_{dves} for bound [^{3}H]vesamicol becomes K_{dves}/β when site B is deprotonated.

Table 2: Equilibrium Saturation Curves for [^{3}H]Vesamicol[a]

pH	K_{dves}^{pH} (nM)[b]	$K_{dves}^{pH7.6}/K_{dves}^{pH}$ [b]
7.1	12.5 ± 1.6	0.80
7.6	10.0 ± 1.3	1.0
8.0	10.9 ± 1.4	0.92
8.9	9.1 ± 1.1	1.1
9.3	5.8 ± 0.7	1.7
10.0	2.1 ± 0.3	4.8

[a]Simultaneous regression to data at the different values of pH was carried out as explained in Appendix 1. The B_{max} value was 40.4 ± 0.5 pmol of hVAChT/mg. [b]For the protonated form of [^{3}H]vesamicol.

DISCUSSION

Terminology. Fundamental mechanisms for binding of protons and other ligands to proteins are understood, but the terminology is not widely known. Thus, we begin the discussion by briefly reviewing some terminology. Consider proton dissociation from an asymmetrical weak diacid, as illustrated in Figure 7. Four states D, E, F, and G are related to each other by "microscopic" acid dissociation constants K_{D1}, K_{D2}, K_{E2}, and K_{F1}. The term microscopic is used here as a chemist uses it to discuss elementary steps in chemical mechanisms, not in the imaging context. If pK_{D1} and pK_{D2} have similar values, states E and F form in similar amounts at intermediate values of pH. At high values of pH, state G predominates. If the acids interact with each other, pK_{E2} and pK_{F1} usually are higher in value than pK_{D1} and pK_{D2}, as electrostatic repulsion between dissociable protons makes loss of the first proton easier than loss of the second proton. If the protonation state of acid A_1H can be monitored, for example by nuclear magnetic resonance spectroscopy, one finds that the pH-titration curve has a complex shape (*30*). In contrast, if pK_{D1} and pK_{D2} have very different values, perhaps because they arise from different types of chemical functionalities like a carboxylic acid and an alkylammonium ion, structures E and F do not form in similar amounts. The pH-titration curve

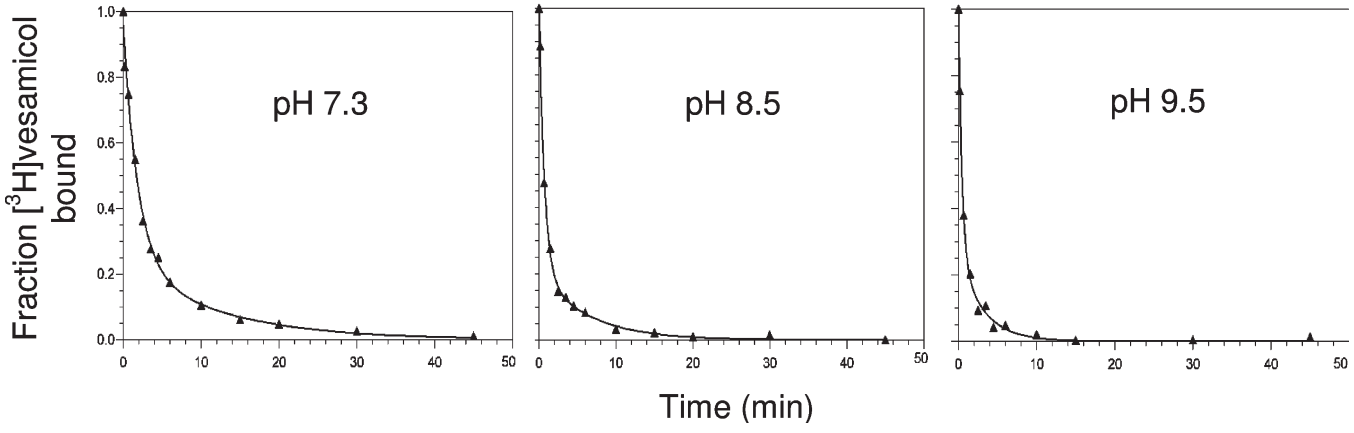

FIGURE 6: Time dependence for dissociation of bound [^{3}H]vesamicol at different pH values. Postnuclear supernatant was incubated with 5 nM [^{3}H]vesamicol for 20 min, and binding was measured, after which a large excess of unlabeled (±)-vesamicol was added. The equation that initially was fitted to each data set is vesamicol bound = B_0fractfast $e^{-k_{fast}t}$ + B_0(1 − fractfast) $e^{-k_{slow}t}$, where the symbols have the apparent meaning and B_0 for each pH was independent of other pH values. Binding was normalized by dividing vesamicol bound values by the B_0 value determined for the same data set so that dissociation rates can be compared with each other visually. Parameter values are in Table 3.

Table 3: Parameters for Biphasic Rates of Dissociation[a]

pH	k_{fast} (min^{-1})	k_{slow} (min^{-1})	fractfast
7.3	0.54 ± 0.08	0.08 ± 0.03	0.75 ± 0.08
8.5	1.42 ± 0.13	0.16 ± 0.05	0.80 ± 0.04
9.5	2.27 ± 0.25	0.33 ± 0.07	0.73 ± 0.05

[a]Similar results were found in one other experiment.

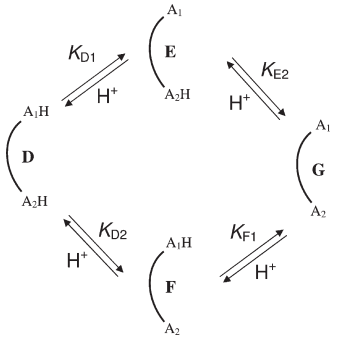

FIGURE 7: Stepwise dissociation of a generalized weak diacid. Different states of acidic dissociation are labeled D−G. The acid dissociation constants are K_{D1}, K_{D2} for the A_1H and A_2H sites in D, respectively, K_{E2} for the A_2H site in E, and K_{F1} for the A_1H site in F. The A_1 and A_2 sites indicated here have no necessary relationship to site A in hVAChT indicated in Figure 5.

for acid A_1H (as well as for acid A_2H) has an ideal shape, even if A_1 and A_2 interact with each other strongly like for glycine. A molecular dissociation constant for loss of the first stoichiometric proton from a diacidic molecule also can be defined, and its value is $\cong K_{D1} + K_{D2}$. A molecular titration can be measured by proton neutralization, and it has an ideal shape for each stoichiometric proton (*31*).

hVAChT contains 88 weakly acidic side chains (total, invariant) [C (7, 1), D (20, 9), E (24, 3), H (8, 1), K (7, 1), Y (22, 7)] that reasonably can have pK values at or below 10. In the VAChT homology model, no R residue is buried or ion paired in a way that might shift its pK value from that of generic R. We assume the 30 R residues have normal pK values of ~12.5 and no R residue titrates significantly in the pH range studied here. Many of the Cs and Ys will not titrate either because they are buried. Although not known exactly, the total number of residues in VAChT that titrate between pH 4 and pH 10 thus is < 88. The number of these that is invariant is only 22, and they are distributed among all six types of candidates. Thus, if additional evidence can be elicited, such as pH-binding profiles for mutants and expectations of conservation due to functional importance, it should be possible eventually to assign pK_1, pK_A, and pK_B to specific residues.

Most of the titratable residues in VAChT will act as isolated acids that do not significantly affect microscopic pK values for other acids (*32*). If an isolated acid interacts strongly with the [^{3}H]vesamicol binding site, affinity for [^{3}H]vesamicol will be pH-dependent and exhibit only slight deviation from an ideal shape due to weak, long-range electrostatic interactions with other residues titrating in the same pH range.

Pairs of acids that interact strongly with each other occur in proteins, particularly at functional sites (*32*). Nevertheless, the equations used here to estimate pK values assume that a detected titration has an ideal shape because it arises from (a) an isolated weak acid, (b) a strongly interacting system having a dominant weak acid, or (c) a system exhibiting molecular-like coupling to the [^{3}H]vesamicol binding site. The assumption is required because the accuracy of the data does not allow further refinement in fitting.

Effects of pH on hVAChT and [^{3}H]Vesamicol. hVAChT and [^{3}H]vesamicol are chemically stable and the filter-binding assay for bound [^{3}H]vesamicol is reliable over the full pH range. A small amount of specific−nonspecific binding that is not VAChT exists in postnuclear supernatant, but it is not quantitatively important in the current experiments. Thus, the experimental system is well behaved.

VAChT and [^{3}H]vesamicol both contain weak acids that affect formation of the complex between them. Although VAChT and [^{3}H]vesamicol are equivalent mathematically in a binding equation, they are not equivalent in structural complexity. [^{3}H]Vesamicol is simple; VAChT is complex. The simplicity of [^{3}H]vesamicol allows computations to account for the effect of proton binding by [^{3}H]vesamicol and reveal additional effects of proton binding by hVAChT.

Five types of pH experiments were conducted here, namely, (a) equilibrium binding by subsaturating [^{3}H]vesamicol, (b) time-dependent adjustment of equilibrium binding, (c) equilibrium saturation curves at multiple acidic pH values, (d) equilibrium saturation curves at multiple basic pH values, and (e) time-dependent dissociation. The experiments provided consistent results that lead to the following conceptual description of [^{3}H]vesamicol binding. Affinity goes toward zero below pH 6 even though [^{3}H]vesamicol does not change its protonation state, as VAChT becomes nonbinding. When pH rises from 7 toward 10, the pH-binding profile has a wiggle shape. The wiggle means that affinity for protonated [^{3}H]vesamicol first decreases slightly and then increases substantially. Despite the increase in intrinsic affinity at pH ~10, the amount of binding goes toward zero as pH increases beyond 10 because the concentration of protonated [^{3}H]vesamicol goes toward zero while the affinity stays constant.

Thermodynamic cycles relate binding of [^{3}H]vesamicol and binding of protons to sites A and B (Figure 5). Binding of [^{3}H]vesamicol increases (or decreases) the dissociation constant for a linked weak acid by the same factor that binding of a proton to the conjugate base increases (or decreases) the dissociation constant for [^{3}H]vesamicol. Thus, pK_A = 7.6 ± 0.2 and pK_B = 10.0 ± 0.1 in free hVAChT become pK_A^{ves} = 7.9 ± 0.3 and pK_A^{ves} = 8.7 ± 0.4 in [^{3}H]vesamicol-bound hVAChT (Table 1). Binding of [^{3}H]vesamicol and a proton to conjugate base A reinforce each other ~2-fold, whereas binding of [^{3}H]vesamicol and a proton to conjugate base B antagonize each other ~18-fold.

Two features in [^{3}H]vesamicol dissociation rates are notable. First, the increase in values of the fast and slow rate constants that occurs at higher pH predicts that equilibrium affinity for [^{3}H]vesamicol should decrease at higher pH, as the rate of dissociation usually is more important than the rate of association in determining equilibrium affinity (*33*). However, the opposite behavior occurs for [^{3}H]vesamicol and hVAChT (Table 2). Second, biphasicity in (−)-vesamicol dissociation rates does not appear in equilibrium saturation curves under any set of conditions tested.

The observations lead to two inferences. The first is that association rates at high pH must increase more than dissociation rates do in order to account for tighter equilibrium binding at higher pH. Indeed, although association is slow enough at pH 7.4 to observe (Figure 3), attempts to observe it at high pH fail

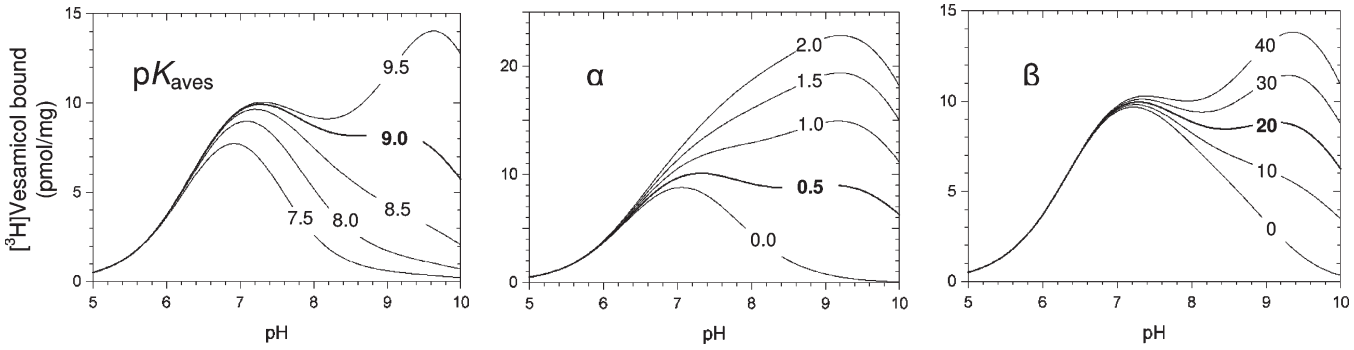

FIGURE 8: Different pK_{aves}, α, and β values in simulated pH-binding profiles for analogues of (−)-vesamicol. Each set of profiles varies the parameter indicated in the upper left corner, and the value of the varied parameter is on top of each profile. The profile and parameter value closest to that of (−)-vesamicol itself in each set are darker. The values of the other parameters are those for (−)-vesamicol listed in Table 1. The concentrations of hVAChT and the analogue of (−)-vesamicol were set at 50 pmol/mg and 5 nM, respectively. The important pH region for PET and SPECT applications is around pH 7.1.

because it becomes too fast for our techniques (not shown). The second inference is that association also must be biphasic and exactly compensate for biphasic dissociation so that equilibrium saturation curves are monophasic. Such behavior suggests that the pathway to and from the [^{3}H]vesamicol binding site exists in open and at least partially closed states. The closed state might be static with reduced, but nonzero, conductance for [^{3}H]vesamicol, or it might be dynamic with zero conductance until it opens to full conductance. The opening would occur at the rate of slow dissociation in the latter case.

Identities and Functions of pK_1, pK_A, and pK_B Acids. They are not known for sure, but clues are accumulating. The pK_1 values for human and rat VAChTs are 6.5 ± 0.1 and 6.28 ± 0.03, respectively (*10*, *16*). Mutation of D398, which resides in the center of TM 10, to an N, A, or E residue very greatly reduces affinity of rat VAChT for [^{3}H]vesamicol (*12*, *13*). This and other data indicate that the [^{3}H]vesamicol binding site probably is located closely to D398 and that D398 might be the source of pK_1. Transport by rat VAChT requires deprotonation of a site with pK_3 = 6.42 ± 0.12 (*12*). Mutation of D398 to N or A, but not E, blocks transport (*12*, *13*). Because of the similarities in pK values and protonation state required for binding and transport, pK_1 and pK_3 likely are due to D398. Aspartic acid, which has a generic pK value of 4.0, can have a value similar to pK_1 and pK_3 in a hydrophobic or negatively charged environment.

Residue E309 originally was thought to be located in loop 7/8 of the hydropathy model for VAChT TMs. For this reason, it was not mutated in prior work. The recently developed homology model relocates TM 7 so that E309 is close to its center and next to D398. This relationship would form a diacid composed of similar chemical functionalities having similar pK values (*9*). Glutamic acid, which has a generic pK value of 4.5, can exhibit pK values in the range of pK_A = 7.6 in a hydrophobic or negatively charged environment. The possible close proximity of E309 to D398 suggests that it too could affect binding of [^{3}H]vesamicol and account for pK_A = 7.6 ± 0.2 and pK_A^{ves} = 7.9 ± 0.3 (*35*). The pK_A and pK_A^{ves} values are similar to pK_4 = 7.56 ± 0.12, which arises from a site that must be protonated for ACh transport (*12*). pK_A, pK_A^{ves}, and pK_4 could arise from the same residue. The relationships among these parameters, E309, and D398 require mutational investigation.

Other residues have been linked by mutations to binding of [^{3}H]vesamicol. They are K131 in the center of TM 2 and D425 in the center of TM 11 (*9*, *12*, *13*, *36*−*38*). Several lines of evidence demonstrate that these residues form an ion pair that ties the first and second bundles of TMs together. An ion pair is a diacid composed of different chemical functionalities that probably have very different pK values. A lysine in such an ion pair is likely to have a pK above generic 10 due to electrostatic stabilization of protonated lysine by the deprotonated aspartate. The pK value for K131 could be too high to appear in any measurement made so far. An aspartic acid in such an ion pair in like manner probably has a pK value below generic 4.5. The pK value for D425 could be too low to appear in any measurement made so far. Although mutations of these two residues have been made and characterized, a clear picture of their functions and likely pK values has not emerged. Neither residue is likely to account for pK_B.

Relevance to PET and SPECT. The (−)-vesamicol family of ligands is being developed for positron emission tomographic (PET) and single-photon computed tomographic (SPECT) applications in human diagnostics (*39*−*41*). Many parameters must be optimized for a successful imaging agent. The current observations suggest that pK_{aves}, α, and β also should be considered, as the VAChT system exhibits plasticity *in vivo*. Binding of several analogues of (−)-vesamicol to *in vivo* striatum increases markedly when ACh turnover increases due to blockade of the D2 receptor (*42*, *43*). In other words, binding of (−)-vesamicol analogues is responsive to indirect pharmacological manipulation in striatum. Could some of the plasticity couple to pK_{aves}, α, and β?

Figure 8 shows computer simulations of pH-binding profiles for different values of pK_{aves}, α, and β. Tomography generally uses ≤half-saturating concentrations of imaging ligand in order to minimize adverse pharmacological effects due to the procedure (*44*). Subsaturation means that changes in the protonation states of hVAChT and the imaging ligand will affect the amount of specific ligand binding and the images obtained. Normal cytoplasmic pH is 7.1 in most human tissues, so we begin the analysis of what different values for pK_{aves}, α, and β could mean at pH 7.1 (*45*, *46*).

The value of pK_{aves} for an imaging ligand will depend on the chemical structure of the ligand. pK_{aves} for (±)-ABV is estimated to be 8.27 ± 0.40, compared to 9.02 ± 0.40 for (±)-vesamicol by the same methodology (*47*). Thus, pK_{aves} indeed probably varies for different analogues of (−)-vesamicol.

A moderate change in pK_{aves} from 9.0 either up or down produces only a small effect on binding to hVAChT at pH 7.1 (Figure 8 left). Values of pK_{aves} < 8.5 decrease binding to hVAChT significantly. Nevertheless, this effect should produce

the same proportional decrease in specific binding throughout an organ that has cytoplasmic pH uniformly at 7.1. An image based on specific binding would not be distorted if sufficient signal were acquired. If regional variation of cytoplasmic pH is not a concern (see below), the value of pK_{aves} is not critical as long as it is not too low.

Different values of α produce significant effects on binding at pH 7.1 as well (Figure 8 center). Nevertheless, like for different values of pK_{aves}, this property of α should not affect images based on specific binding if the cytoplasm throughout an organ is uniformly at pH 7.1 and sufficient data are obtained. Different values for the parameter β have very little effect on binding and should have very little effect on images acquired at pH 7.1 (Figure 8 right).

The potential importance of pK_{aves}, α, and β is greater if the cytoplasmic pH in different regions of an imaged organ differs due to pathology or dynamic physiology. The remaining discussion will be restricted to the realistic pH range of 6.6−7.3 (*45*, *46*). A small change in pH of < 0.1 either up or down from normal has little effect on binding for all values of pK_{aves}, as there always is a peak in the pH-binding profile near pH 7.1 (Figure 8 left). In contrast, a drop in pH to 6.6 causes 21% decreased binding of a ligand with pK_{aves} = 9.0. The decrease primarily is due to pK_1 in hVAChT, which is fixed in value. Nevertheless, the decrease in binding that occurs from pH 7.1 to pH 6.6 can be minimized by ligand design. It is smaller when pK_{aves} is lower. The peak of binding around pH 7.1 is lower, but the amount of binding at more acidic pH is not. Thus, lower pK_{aves} values should produce less distortion of images by regional acidification. In the case of regional alkalization, which cannot be severe, a quite small difference in binding should occur if pK_{aves} is > 8.5, due to the presence of the shoulder on the high-pH side of the binding peak. A larger decrease would occur during alkalization if pK_{aves} is ≤8.0, as the shoulder disappears. Control of pK_{aves} during ligand design can minimize the effect of either regional acidification or regional alkalization but not both in a single imaging agent. In most cases, lower pK_{aves} would be desirable.

The parameters α and β quantitatively express the extent of coupling between bound ligand and the protonation states of sites A and B. Their values almost surely depend on the structure of the ligand, although this expectation has not been tested. When α is 0 to 0.5, the pH-binding profile exhibits a peak (or peak and high-pH shoulder) that makes binding insensitive to small deviations up or down from pH 7.1 (Figure 8 center). However, acidification to pH 6.6 produces a significant decrease in binding at all values of α. By an analysis similar to that used for pK_{aves}, α ≤ 0.5 should produce less distortion of images. When α ≥ 1.0 the high-pH shoulder becomes dominant. The pH-binding profile takes on a steep positive slope at pH 7.1 that produces a large change in binding when a small change either up or down in pH occurs. A ligand with α ≥ 1.0 is not desirable, as it would produce distortions in images when cytoplasmic pH differs in different regions of an organ. Instead, lower α would be desirable.

All values of β show a peak around pH 7.1 that produces low sensitivity to moderate differences in pH either up or down. Large acidification causes a large decrease in binding that cannot be mitigated by adjusting β through ligand design. The β parameter is of lesser utility for designing PET and SPECT ligands.

Similar Transporters. Vesicular monoamine transporters (VMATs) 1 and 2 have amino acid sequences, biochemical mechanisms, and pH-transport profiles similar to those of VAChT (*48*). They store the monoamine family of neurotransmitters (dopamine, serotonin, and so on) in secretory vesicles and granules. The residues corresponding to E309, D398, and D425 in hVAChT are of the same invariant types in VMATs. VMAT 2 is inhibited by tetrabenazine, which binds with a pH profile similar to that of [^{3}H]vesamicol binding to VAChT (*49*, *50*). As for [^{3}H]vesamicol, the binding is complicated by deprotonation of a tertiary alkylamine. Reserpine is another potent inhibitor of VMATs containing a tertiary alkylamine. Both inhibitors are used for PET imaging in human beings (*51*, *52*). The analysis methods here might be of use in understanding proton-binding sites in VMATs and the potential complications and opportunities they bring to imaging.

APPENDIX

(*1*) [^{3}*H*]*Vesamicol Saturation Curves at Different pH Values*. Equation 1 gives nonspecific binding ($bound^{pH}_{nonspecific}$ in pmol/mg) at any particular pH, and eq 2 gives total binding ($bound^{pH}_{total}$ in pmol/mg) at any particular pH.

$$bound^{pH}_{nonspecific} = m^{pH}V \quad (1)$$

$$bound^{pH}_{total} = B_{max}VF_{ves}/(K^{pH}_{dves}+VF_{ves})+bound^{pH}_{nonspecific} \quad (2)$$

V is the concentration of free [^{3}H]vesamicol in nanomolar, B_{max} is the picomoles per milligram of [^{3}H]vesamicol binding to VAChT at saturation, K^{pH}_{dves} is the dissociation constant in nanomolar for protonated [^{3}H]vesamicol at a particular pH, and F_{ves} is the fraction of protonated [^{3}H]vesamicol given by eq 3. Only protonated [^{3}H]vesamicol is assumed to bind.

$$F_{ves} = 10^{-pH}/(10^{-pH}+10^{-pK_{aves}}) \quad (3)$$

pK_{aves} is the negative logarithm of the acid dissociation constant for protonated [^{3}H]vesamicol, which has been estimated to be 9.0 ± 0.1 by the more accurate of two methods that both arrived at pK_{aves} = 9.0 (*19*, *47*). Initial fits demonstrated that [^{3}H]vesamicol affinity increases enough at high pH that free [^{3}H]vesamicol (V) is significantly less than total [^{3}H]vesamicol (V_{tot}), as given by eq 4.

$$V = V_{tot} - conc \times bound^{pH}_{tot} \quad (4)$$

Concentration (conc) in milligrams per milliliter converts picomoles per milligram of bound [^{3}H]vesamicol into nanomolar bound [^{3}H]vesamicol. It was 0.1 mg/mL in the current experiment. Substitution of eq 2 into eq 4 generates a quadratic equation with two roots for V. The appropriate root is $0 < V < V_{tot}$. Substitution of V into eqs 1 and 2 produces two equations in the independent variables V_{tot} and pH and the adjustable parameters B_{max}, K^{pH}_{dves}, and m^{pH}. Superscript pH in the names of parameters and dependent variables is an identifier, not an exponent. The parameter m^{pH} is not of biological significance. A data file for each pH value was generated containing total and nonspecific binding in the presence of zero to high concentrations of V_{tot}. Equations 1−4 were replicated for each pH value, and the pH was specified in each set of eqs 1−4 for the parameters and dependent variables of that set, for example, $bound^{pH7.1}_{nonspecific}$, $m^{pH7.1}$, $bound^{pH7.1}_{total}$, and $K^{pH7.1}_{dves}$. Thus, six variations of eqs 1−4 were fitted simultaneously to the six merged data files using a common B_{max} value with pK_{aves} fixed to its independently determined value of 9.0 (*19*). The results for K^{pH}_{dves} at each pH are listed in Table 2.

(*2*) *hVAChT Protonation Model*. Preferred model iii in the text (Figure 5) assumes that when (a) protonation of site 1 having pK_1 occurs, [^{3}H]vesamicol cannot bind, (b) deprotonation of site B having pK_B increases [^{3}H]vesamicol affinity, and (c) deprotonation of site A having pK_A decreases affinity. Derivation of an expression that can be fitted to the data in Figure 1 begins with global eq 5.

$$\text{vesamicol bound} = B_{max}\text{VAChT}_{bound}/(\text{VAChT}_{free}+\text{VAChT}_{bound}) \quad (5)$$

Vesamicol bound gives the amount of [^{3}H]vesamicol bound to VAChT at any pH value. VAChT_{free} is equal to the sum of all forms of transporter not bound to [^{3}H]vesamicol given by eq 6.

$$\begin{aligned}\text{VAChT}_{free} &= \text{VAChT}\cdot\text{H}_A{}^+\cdot\text{H}_B{}^+ + \text{VAChT}\cdot\text{H}_A{}^+ \\ &+ \text{VAChT}\cdot\text{H}_B{}^+ + \text{VAChT} + \text{H}_1{}^+\cdot\text{VAChT}\cdot\text{H}_A{}^+\cdot\text{H}_B{}^+ \\ &+ \text{H}_1{}^+\cdot\text{VAChT}\cdot\text{H}_A{}^+ + \text{H}_1{}^+\cdot\text{VAChT}\cdot\text{H}_B{}^+ \quad (6)\end{aligned}$$

Because VAChT deprotonated at both sites A and B exists at only high pH where protonation at site 1 is negligible, we ignore $\text{H}_1{}^+\cdot$VAChT. Assume that the concentration of VAChT dominant at neutral pH (namely, $\text{VAChT}\cdot\text{H}_A{}^+\cdot\text{H}_B{}^+$) is 1. The concentrations of the [^{3}H]vesamicol-free states then are given by eqs 7−13.

$$\text{VAChT}\cdot\text{H}_A{}^+\cdot\text{H}_B{}^+ = 1 \quad (7)$$

$$\text{VAChT} = 10^{2\text{pH}-\text{p}K_A-\text{p}K_B} \quad (8)$$

$$\text{VAChT}\cdot\text{H}_A{}^+ = 10^{\text{pH}-\text{p}K_B} \quad (9)$$

$$\text{VAChT}\cdot\text{H}_B{}^+ = 10^{\text{pH}-\text{p}K_A} \quad (10)$$

$$\text{H}_1{}^+\cdot\text{VAChT}\cdot\text{H}_A{}^+\cdot\text{H}_B{}^+ = 10^{\text{p}K_1-\text{pH}} \quad (11)$$

$$\text{H}_1{}^+\cdot\text{VAChT}\cdot\text{H}_A{}^+ = 10^{\text{p}K_1-\text{p}K_B} \quad (12)$$

$$\text{H}_1{}^+\cdot\text{VAChT}\cdot\text{H}_B{}^+ = 10^{\text{p}K_1-\text{p}K_A} \quad (13)$$

The expressions on the right sides of eqs 7−13 are substituted into eq 6. VAChT_{bound} is equal to the sum of all forms of transporter bound to [^{3}H]vesamicol as given by eq 14. Only protonated [^{3}H]vesamicol is assumed to bind.

$$\begin{aligned}\text{VAChT}_{bound} &= \text{VH}^+\cdot\text{VAChT}\cdot\text{H}_A{}^+\cdot\text{H}_B{}^+ \\ &+ \text{VH}^+\cdot\text{VAChT}\cdot\text{H}_A{}^+ + \text{VH}^+\cdot\text{VAChT}\cdot\text{H}_B{}^+ + \text{VH}^+\cdot\text{VAChT} \quad (14)\end{aligned}$$

The concentrations of the [^{3}H]vesamicol-bound states are given by eqs 15−18. K_{dves} is the "pH-independent" [^{3}H]vesamicol dissociation constant for the $\text{VH}^+\cdot\text{VAChT}\cdot\text{H}_A{}^+\cdot\text{H}_B{}^+$ complex.

$$\text{VH}^+\cdot\text{VAChT}\cdot\text{H}_A{}^+\cdot\text{H}_B{}^+ = F_{ves}V/K_{dves} \quad (15)$$

$$\text{VH}^+\cdot\text{VAChT}\cdot\text{H}_B{}^+ = F_{ves}V\alpha \times 10^{\text{pH}-\text{p}K_A}/K_{dves} \quad (16)$$

$$\text{VH}^+\cdot\text{VAChT}\cdot\text{H}_A{}^+ = F_{ves}V\beta \times 10^{\text{pH}-\text{p}K_B}/K\text{dves} \quad (17)$$

$$\text{VH}^+\cdot\text{VAChT} = F_{ves}V\alpha\beta \times 10^{2\text{pH}-\text{p}K_A-\text{p}K_B}/K_{dves} \quad (18)$$

Equation 3 in Appendix 1 is substituted for F_{ves} in eqs 15−18. The amount of [^{3}H]vesamicol binding is small enough to ignore, so V_{tot} (namely, a constant 5 nM) will be taken as V. The expressions on the right sides of eqs 15−18 are substituted into eq 14. Equations 6 and 14 then are substituted into global eq 5, which yields an equation in the dependent variable vesamicol bound, the independent variable pH, and the adjustable parameters pK_1, pK_A, α, pK_B, β, and K_{dves}. The values of B_{max} and pK_{aves} were fixed at their independently determined values for regression to pH-binding data of the sort shown in Figure 1.

REFERENCES

1. Parsons, S. M., Prior, C., and Marshall, I. G. (1993) Acetylcholine transport, storage, and release. *Int. Rev. Neurobiol. 35*, 279–390.
2. Usdin, T. B., Eiden, L. E., Bonner, T. I., and Erickson, J. D. (1995) Molecular biology of the vesicular ACh transporter. *Trends Neurosci. 18*, 218–224.
3. Saier, M. H. J., Beatty, J. T., Goffeau, A., Harley, K. T., Heijne, W. H., Huang, S. C., Jack, D. L., Jahn, P. S., Lew, K., Liu, J., Pao, S. S., Paulsen, I. T., Tseng, T. T., and Virk, P. S. (1999) The major facilitator superfamily. *J. Mol. Microbiol. Biotechnol. 1*, 257–79.
4. Abramson, J., Smirnova, I., Kasho, V., Verner, G., Kaback, H. R., and Iwata, S. (2003) Structure and mechanism of the lactose permease of *Escherichia coli*. *Science 301*, 610–615.
5. Huang, Y., Lemieux, M. J., Song, J., Auer, M., and Wang, D. N. (2003) Structure and mechanism of the glycerol-3-phosphate transporter from *Escherichia coli*. *Science 301*, 616–620.
6. Hirai, T., Heymann, J. A. W., Shi, D., Sarker, R., Maloney, P. C., and Subramaniam, S. (2002) Three-dimensional structure of a bacterial oxalate transporter. *Nat. Struct. Mol. Biol. 9*, 597–600.
7. Yin, Y., He, X., Szewczyk, P., Nguyen, T., and Chang, G. (2006) Structure of the multidrug transporter EmrD from *Escherichia coli*. *Science 312*, 741–744.
8. Law, C. J., Maloney, P. C., and Wang, D. N. (2008) Ins and outs of major facilitator superfamily antiporters. *Annu. Rev. Microbiol. 62*, 289–305.
9. Vardy, E., Arkin, I. T., Gottschalk, K. E., Kaback, H. R., and Schuldiner, S. (2004) Structural conservation in the major facilitator superfamily as revealed by comparative modeling. *Protein Sci. 13*, 1832–1840.
10. Nguyen, M. L., Cox, G. D., and Parsons, S. M. (1998) Kinetic parameters for the vesicular acetylcholine transporter: two protons are exchanged for one acetylcholine. *Biochemistry 37*, 13400–13410.
11. Bahr, B. A., and Parsons, S. M. (1986) Acetylcholine transport and drug inhibition kinetics in *Torpedo* synaptic vesicles. *J. Neurochem. 46*, 1214–1218.
12. Bravo, D. T., Kolmakova, N. G., and Parsons, S. M. (2005) Mutational and pH analysis of ionic residues in transmembrane domains of vesicular acetylcholine transporter. *Biochemistry 44*, 7955–7966.
13. Kim, M. H., Lu, M., Lim, E. J., Chai, Y. G., and Hersh, L. B. (1999) Mutational analysis of aspartate residues in the transmembrane regions and cytoplasmic loops of rat vesicular acetylcholine transporter. *J. Biol. Chem. 274*, 673–680.
14. Ojeda, A. M., Kolmakova, N. G., and Parsons, S. M. (2004) Acetylcholine binding site in the vesicular acetylcholine transporter. *Biochemistry 43*, 11163–11174.
15. D'rozario, R. S. G., and Sansom, M. S. P. (2008) Helix dynamics in a membrane transport protein: comparative simulations of the glycerol-3-phosphate transporter and its constituent helices. *Mol. Membr. Biol. 25*, 571–583.
16. Kornreich, W. D., and Parsons, S. M. (1988) Sidedness and chemical and kinetic properties of the vesamicol receptor of cholinergic synaptic vesicles. *Biochemistry 27*, 5262–5267.
17. Dixon, M., and Webb, E. C. (1964) Enzymes , pp 128−145, Longmans, London.
18. Rogers, G. A., Parsons, S. M., Anderson, D. C., Nilsson, L. M., Bahr, B. A., Kornreich, W. D., Kaufman, R., Jacobs, R. S., and Kirtman, B. (1989) Synthesis, *in vitro* acetylcholine-storage-blocking activities, and biological properties of derivatives and analogues of *trans*-2-(4-phenylpiperidino)cyclohexanol (vesamicol). *J. Med. Chem. 32*, 1217–1230.
19. Bravo, D. T., and Parsons, S. M. (2009) pK_a of vesamicol, unpublished work.
20. Shimojo, M., Wu, D., and Hersh, L. B. (1998) The cholinergic gene locus is coordinately regulated by protein kinase A II in PC12 cells. *J. Neurochem. 71*, 1118–1126.
21. Bonzelius, F., Herman, G., Cardone, M., Mostov, K., and Kelly, R. (1994) The polymeric immunoglobulin receptor accumulates in specialized endosomes but not synaptic vesicles within the neurites of transfected neuroendocrine PC12 cells. *J. Cell Biol. 127*, 1603–1616.

22. Khare, P., White, A. R., Mulakaluri, A., and Parsons, S. M. (2009) Equilibrium binding and transport characterization of vesicular acetylcholine transporter, Methods Mol. Biol. (in press).
23. Bradford, M. M. (1976) A rapid and sensitive method for the quantitation of microgram quantities of protein utilizing the principle of protein-dye binding. *Anal. Biochem. 72*, 248–254.
24. Varoqui, H., and Erickson, J. D. (1996) Active transport of acetylcholine by the human vesicular acetylcholine transporter. *J. Biol. Chem. 271*, 27229–27232.
25. Keller, J. E., and Parsons, S. M. (2000) A critical histidine in the vesicular acetylcholine transporter. *Neurochem. Int. 36*, 113–117.
26. Rogers, G. A., Kornreich, W. D., Hand, K., and Parsons, S. M. (1993) Kinetic and equilibrium characterization of vesamicol receptor ligand complexes with picomolar dissociation constants. *Mol. Pharmacol. 44*, 633–641.
27. Efange, S. M., Mach, R. H., Smith, C. R., Khare, A. B., Foulon, C., Akella, S. K., Childers, S. R., and Parsons, S. M. (1995) Vesamicol analogues as sigma ligands. Molecular determinants of selectivity at the vesamicol receptor. *Biochem. Pharmacol. 49*, 791–797.
28. Sagi, N., Yamamoto, H., Yamamoto, T., Okuyama, S., and Moroji, T. (1996) Possible expression of a σ1 site in rat pheochromocytoma (PC12) cells. *Eur. J. Pharmacol. 304*, 185–190.
29. Compute pI/Mw tool.http://ca.expasy.org/tools/pi_tool.html, accessed Feb 5, 2009.
30. Szakács, Z., Kraszni, M., and Noszál, B. (2004) Determination of microscopic acid−base parameters from NMR−pH titrations. *Anal. Bioanal. Chem. 378*, 1428–1448.
31. Holmes, D. L., and Lightner, D. A. (1996) Synthesis and acidity constants of $^{13}CO_2H$-labelled dicarboxylic acids. pK_as from ^{13}C-NMR. *Tetrahedron 52*, 5319–5338.
32. Brocklehurst, K. (1994) A sound basis for pH-dependent kinetic studies on enzymes. *Protein Eng. 7*, 291–299.
33. Josée, E., Leysen, and Gommeren, W. (1986) Drug-receptor dissociation time, new tool for drug research: Receptor binding affinity and drug-receptor dissociation profiles of serotonin, dopamine, histamine, antagonists, and opiates. *Drug Dev. Res. 8*, 119–131.
34. Zhu, H., Duerr, J. S., Varoqui, H., McManus, J. R., Rand, J. B., and Erickson, J. D. (2001) Analysis of point mutants in the *Caenorhabditis elegans* vesicular acetylcholine transporter reveals domains involved in substrate translocation. *J. Biol. Chem. 276*, 41580–41587.
35. Khare, P., Ojeda, A. M., Chandrasekaran, A., and Parsons, S. M. (2007) Interacting acidic residues in transmembrane segments of vesicular acetylcholine transporter, Poster abstract 579.18/M27, Society for Neuroscience Conference, San Diego.
36. Kim, M. H., Lu, M., Kelly, M., and Hersh, L. B. (2000) Mutational analysis of basic residues in the rat vesicular acetylcholine transporter. Identification of a transmembrane ion pair and evidence that histidine is not involved in proton translocation. *J. Biol. Chem. 275*, 6175–6180.
37. Merickel, A., Kaback, H. R., and Edwards, R. H. (1997) Charged residues in transmembrane domains II and XI of a vesicular monoamine transporter form a charge pair that promotes high affinity substrate recognition. *J. Biol. Chem. 272*, 5403–5408.
38. Bahr, B. A., Clarkson, E. D., Rogers, G. A., Noremberg, K., and Parsons, S. M. (1992) A kinetic and allosteric model for the acetylcholine transporter−vesamicol receptor in synaptic vesicles. *Biochemistry 31*, 5752–5762.
39. Volkow, N. D., Ding, Y.-S., Fowler, J. S., and Gatley, S. J. (2001) Imaging brain cholinergic activity with positron emission tomography: its role in the evaluation of cholinergic treatments in Alzheimer's dementia. *Biol. Psychiat. 49*, 211–220.
40. Langer, O., and Halldin, C. (2002) PET and SPET tracers for mapping the cardiac nervous system. *Eur. J. Nucl. Med. Mol. I 29*, 416–434.
41. Tu, Z., Efange, S. M. N., Xu, J., Li, S., Jones, L. A., Parsons, S. M., and Mach, R. H. (2009) Synthesis and *in vitro* and *in vivo* evaluation of ^{18}F-labeled positron emission tomography (PET) ligands for imaging the vesicular acetylcholine transporter. *J. Med. Chem. 52*, 1358–1369.
42. Ingvar, M., Stone-Elander, S., Rogers, G. A., Johansson, B., Eriksson, L., Parsons, S. M., and Widen, L. (1993) Striatal D2/acetylcholine interactions: PET studies of the vesamicol receptor. *NeuroReport 4*, 1311–1314.
43. Efange, S. M. N., Langason, R. B., and Khare, A. B. (1996) Age-related diminution of dopamine antagonist-stimulated vesamicol receptor binding. *J. Nucl. Med. 37*, 1192–1197.
44. Holden, J. E., and Doudet, D. J. (2004) Positron emission tomography receptor assay with multiple ligand concentrations: an equilibrium approach. *Methods Enzymol. 385* (Imaging Biol. Res., Part A), 169–184.
45. Kintner, D. B., Anderson, M. K., Fitzpatrick, J. H. Jr., Sailor, K. A., and Gilboe, D. D. (2000) ^{31}P-MRS-based determination of brain intracellular and interstitial pH: its application to *in vivo* H^+ compartmentation and cellular regulation during hypoxic/ischemic conditions. *Neurochem. Res. 25*, 1385–1396.
46. Grafe, P. (1998) Abnormal cytoplasmic pH in diseases of nerve and muscle, in pH and Brain Function (Kaila, K., and Ransom, B. R., Eds.) pp 621−628, Wiley-Liss, New York.
47. SciFinder Scholar of the Chemical Abstracts Service quotes a pK_a value of 9.02 ± 0.40 for (±)-vesamicol and 8.27 ± 0.40 for (±)-ABV as estimated by Advanced Chemistry Development using Software V8.14 for Solaris (1994−2009 by ACD/Laboratories).
48. Parsons, S. M. (2000) Transport mechanisms in acetylcholine and monoamine storage. *FASEB J. 14*, 2423–2434.
49. Scherman, D., and Henry, J. (1983) The catecholamine carrier of bovine chromaffin granules. Form of the bound amine. *Mol. Pharmacol. 23*, 431–436.
50. Scherman, D. H., and Henry, Jean Pierre (1982) Acid-base properties of the catecholamine uptake inhibitors tetrabenazine and dihydrotetrabenazine. *Biochimie 64*, 915–921.
51. Brooks, D. J., Frey, K. A., Marek, K. L., Oakes, D., Paty, D., Prentice, R., Shults, C. W., and Stoessl, A. J. (2003) Assessment of neuroimaging techniques as biomarkers of the progression of Parkinson's disease. *Exp. Neurol. 184* (Suppl. 1), S68–S79.
52. Ravina, B., Eidelberg, D., Ahlskog, J. E., Albin, R. L., Brooks, D. J., Carbon, M., Dhawan, V., Feigin, A., Fahn, S., Guttman, M., Gwinn-Hardy, K., McFarland, H., Innis, R., Katz, R. G., Kieburtz, K., Kish, S. J., Lange, N., Langston, J. W., Marek, K., Morin, L., Moy, C., Murphy, D., Oertel, W. H., Oliver, G., Palesch, Y., Powers, W., Seibyl, J., Sethi, K. D., Shults, C. W., Sheehy, P., Stoessl, A. J., and Holloway, R. (2005) The role of radiotracer imaging in Parkinson disease. *Neurology 64*, 208–215.